Am J Cancer Res 2024;14(5):2141-2156
www.ajcr.us /ISSN:2156-6976/ajcr0155263

Original Article

Cancer-associated MDM2 W329G mutant attenuates ribosomal stress-mediated p53 responses to promote cell survival and glycolysis

Sally Lien[1], Thomas P Whitbread[1*], Shiva O Shastri[1*], Jamie A Contreras[1], Ruiying Zhao[2], Yan Zhu[1]

[1]Department of Biological Sciences, St. John's University, Queens, NY 11439, USA; [2]Department of Integrative Biology and Pharmacology, McGovern Medical School, The University of Texas Health Science Center at Houston, Houston, TX 77030, USA. [*]Equal contributors.

Received January 3, 2024; Accepted February 4, 2024; Epub May 15, 2024; Published May 30, 2024

Abstract: Although amplification/overexpression is the predominant mechanism for the oncogenic properties of MDM2, an increasing number of MDM2 somatic missense mutations were identified in cancer patients with the recent advances in sequencing technology. Here, we characterized an MDM2 cancer-associated mutant variant W329G identified from a patient sample that contains a wild-type p53 gene. Trp329 is one of residues that were reported to be critical to MDM2's binding to ribosomal protein L11 (RPL11). We found that the MDM2 W329G mutant was resistant to the inhibitory effect of RPL11 on MDM2-mediated p53 ubiquitination and degradation, in line with its defect on RPL11 binding. Using isogenic U2OS cells with or without endogenous MDM2 W329G mutation, we demonstrated that the expression of classic p53 targets induced by ribosomal stress signals was reduced in mutant cells. RNA-seq analysis revealed that upon 5-FU treatment, the p53 response was significantly impaired. Also, the 5-FU-mediated repression of genes in cell cycle progression and DNA replication was diminished in W329G mutant-containing cells. Physiologically, U2OS W329G cells were more resistant to cell growth inhibition induced by ribosomal stress and exhibited higher glycolytic rates upon 5-FU treatment. Together, our data indicated that cancer-associated MDM2 W329G mutant attenuates ribosomal stress-mediated p53 responses to promote cell survival and glycolysis.

Keywords: MDM2, p53, cancer-associated mutations, ribosomal stress

Introduction

MDM2 is a crucial negative regulator of p53, the most commonly mutated tumor suppressor in cancer. In response to various cellular stresses, active p53 protein is released from MDM2 to regulate numerous effectors involved in cell cycle arrest, apoptosis, senescence, and differentiation [1-3]. MDM2 binds directly to the N-terminal transactivation domain of p53 and modulates the function of p53 through several mechanisms, including inhibition of p53-dependent transcription, facilitation of p53 proteasome degradation by an E3 ubiquitin ligase activity, and translocation of p53 from nucleus to cytoplasm [4]. In turn, the p53 protein binds to the promoter of MDM2 and activates MDM2 transcription. The feedback loop between MDM2 and p53 fine-tunes the cellular responses after p53 activation. Loss of the *Mdm2* gene in mice results in early embryonic lethality, whereas deletion of the *p53* gene with the *Mdm2* gene rescues the lethal phenotype [5]. MDMX (also referred to as MDM4) is the MDM2 homolog and another crucial negative regulator of p53. It has been shown that MDMX inhibits the p53 function mainly by repressing its transcriptional activity [6]. MDMX lacks the E3 ubiquitin ligase activity [7] but has been reported to promote MDM2-mediated p53 degradation through MDM2/MDMX heterodimer formation [8-11]. Overexpression of MDMX has been documented in different types of human cancers [12]. Loss of *Mdmx* in mice also leads to embryonic lethality and deletion of *p53* with *Mdmx* rescues the lethal phenotype [13, 14].

MDM2 gene is amplified and overexpressed in various human cancers, especially in the tumors that retain wild-type p53, although over-

https://doi.org/10.62347/QIFC4021

expression of MDM2 is not mutually exclusive with mutation of p53 [15]. Amplification of MDM2 gene is sufficient in and of itself to induce the broad range of tumor types and the numbers of tumors [16]. Targeting MDM2 has been considered a promising treatment strategy, and an increasing number of MDM2 inhibitors are under preclinical and clinical investigation [17, 18]. Advances in sequencing technology have enabled a comprehensive dissection of the cancer genome and led to the identification of a significantly increasing number of somatic mutations that are involved in cancer [19]. Intriguingly, MDM2 mutations are rare in cancer. A single nucleotide polymorphism (SNP309) was found in the *MDM2* promoter and has been shown to associate with accelerated tumor formation in both hereditary and sporadic cancers in humans [20]. Among several reported MDM2 somatic mutants, one variant (MDM2 C305F) was found to accelerate Eμ-*Myc*-induced lymphomagenesis in mice and showed defects in the normal metabolic response when subjected to calorific restriction [21, 22]. Several cancer-associated MDM2 mutants have been characterized using ectopically overexpressed proteins, although contradictory results have been obtained for some mutants [23, 24]. In addition, several lab-engineered mutations targeting residues at critical functional domains of MDM2 have been reported mainly using overexpressing assays [25, 26]. Although those studies have provided valuable information on understanding the oncogenic function of MDM2, it would be interesting to confirm those findings under a physiological setting and test the concept that specific MDM2 mutations (especially those residing in critical functional domains of MDM2) can function as driver mutations for tumorigenesis.

We analyzed the COSMIC (Catalogue Of Somatic Mutations In Cancer) database for MDM2 mutations that are associated with cancer, with particular interest in the MDM2 cancer-associated mutations that occur at functional domains of MDM2 as they may be the driver mutations leading to tumorigenesis. Various factors have shown that perturbation of ribosomal biogenesis generates ribosomal stress that causes ribosome-free forms of RPs' (notably RPL11) interaction with MDM2, resulting in p53 stabilization and activation [27, 28]. The RP-MDM2-p53 surveillance network monitors the fidelity of ribosomal biogenesis and serves as a crucial tumor-suppression mechanism [4, 29]. The structure of MDM2 in complex with RPL11 has been reported [30], and multiple cancer-associated MDM2 mutations identified in the COSMIC database happen on residues involved in MDM2-RPL11 interaction. MDM2-binding RPL11-mimetics have been reported to target the RPL11-MDM2-p53 pathway for anticancer therapeutics [31]. Here, we chose an MDM2 cancer-associated mutant variant, W329G, identified from a patient sample that contains a wild-type p53 gene for further characterization. Trp329 is one of the residues that are important for MDM2-RPL11 binding. To examine the function of MDM2 W329G and its role in tumorigenesis under a physiological setting, we established cell lines with W329G at the endogenous MDM2 gene locus using CRISPR/Cas9-based genome editing methods. Our results indicate that the MDM2 W329G variant attenuates p53-mediated cellular responses to ribosomal stress to promote cell survival.

Material and methods

Plasmids and cell culture

Flag-MDM2 (wild-type), HA-p53, pCMV-p53, Myc-MDMX, Myc-L11, and HA-Ubiquitin were described previously [32]. Flag-MDM2 (W329G) was constructed by site-directed mutagenesis using Flag-MDM2 as a template. The mutation was confirmed by Sanger sequencing.

U2OS cells (osteosarcoma cells expressing wild-type p53) and H1299 cells (p53-null lung epithelial carcinoma cells) were grown in Dulbecco modified Eagle medium containing 10% fetal bovine serum (Gemini) plus 1% penicillin-streptomycin (Gibco) at 37°C, 5% CO_2.

Isogenic U2OS wild-type and MDM2 W329G cells were generated using CRISPR/Cas9 genome-editing technology [33]. The left (anti-sense; GTTGCAATGTGATGGAAGGG) and right (sense; GTTGGGCCCTTCGTGAGAATTGG) sgRNAs were cloned into pX335 (Addgene #42335) to cut the genome DNA in the exon 11 of the *MDM2* gene. The donor vector was designed to introduce mutation W329G (TGG to GGG) in exon 11 of the *MDM2* gene with a FNF selection cassette flanked by left and right homologous arms and cloned into pFNF

(Addgene #22687). The donor and CRISPR plasmids were transfected into U2OS cells, followed by selection with G418 (800 μg/ml) for 2 to 3 weeks. The resistant clones were expanded and examined by PCR for FNF insertion on the *MDM2* gene locus. The corrected clones were confirmed by both genome and cDNA sequencing. Isogenic wild-type clones were also obtained through the same selection process to serve as controls. All the clones were maintained in Dulbecco-modified Eagle medium containing 10% fetal bovine serum, 1% penicillin-streptomycin, and 250 μg/ml G418.

U2OS shRNA p53 knockdown and shRNA control cells were generated using a lentivirus shRNA knockdown vector system. Lentiviral particles containing shRNAs targeting p53 (pLKO-p53-shRNA-427; Addgene #25636 and pLKO-p53-shRNA-941; Addgene #25637) [34] as well as control shRNAs (pLKO.pig Luc shRNA and pLKO.pig control shRNA1) [35, 36] were produced in HEK293T cells and subsequently delivered to isogenic U2OS wild-type or MDM2 W329G cells following Addgene pLKO.1 Protocol. 2 μg/ml of puromycin was added to the transduced plates two days after infection for selecting stable clones. Five days after selection, cells were harvested to determine the p53 protein levels. Control or p53 knock-down cells were maintained in Dulbecco-modified Eagle medium containing 10% fetal bovine serum, 1% penicillin-streptomycin, and 2 μg/ml puromycin. When needed, they were pooled right before plating for the experiments.

Antibodies and drugs

Commercially obtained antibodies were used to detect the following proteins or epitopes: human p53 (rabbit polyclonal antibody; FL393, Santa Cruz), c-Myc (monoclonal antibody; 9E10, Santa Cruz), Flag (mouse monoclonal antibody; M2, Sigma), HA (mouse monoclonal antibody; HA.11, Biolegend), GFP (mouse monoclonal antibody; B-2, Santa Cruz), p21 (rabbit monoclonal antibody; 12D1, Cell signaling), MDMX (monoclonal antibody; 8C6, Millipore), MDM2 (rabbit polyclonal antibody; N-20, Santa Cruz), E2F1 (mouse monoclonal antibody; KH95, Santa Cruz), RPL11 (rabbit polyclonal antibody; PA5-34604, Invitrogen). Mouse monoclonal antibodies against human p53 (DO-1) and MDM2 (3G5, 4B11, 5B10) were used as supernatants from hybridoma cultures. Drugs used in this study are as follows: 5-FU (50 μM; Sigma), MG132 (20 μM; Calbiochem), Actinomycin D (5 nM; Sigma), G418 (250 or 800 μg/ml; Gemini), Puromycin (2 μg/ml; InvivoGen).

Transfections and immunoblotting

Transfections were performed using Lipofectamine 2000 (Invitrogen) according to the manufacturer's instructions. In all transfection experiments, balancing amounts of empty vector (pcDNA3 plasmid) were added to ensure equal amounts of total DNA used for transfecting cells. Cells were lysed with TEB Lysis Buffer (10 mM Tris-Hcl pH 7.5, 150 mM NaCl, 10% glycerol, and 1% Nonidet P-40 with 50 nM PMSF and protease inhibitor cocktail (sigma; S8820). After 10,000-rpm centrifugation at 4°C for 10 minutes, total cleared cell lysates were collected, and protein concentration was measured using the Bradford assay (Bio-Rad). Equivalent lysates were separated by SDS-PAGE, transferred onto nitrocellulose membranes, and blocked with PBS containing 0.1% Tween 20 (Sigma) and 2% non-fat dry milk for 1 hour. Then antibodies were applied, and Digital-ECL Substrate (Kindle Bioscience) was used for protein visualization with KwikQuant Imager (Kindle Bioscience).

Immunofluorescent staining

U2OS cells grown on coverslips were transfected with 1 μg of Flag-tagged MDM2 (wild-type or W329G). Twenty-four hours after transfection, cells were fixed by 4% paraformaldehyde in PBS and then subjected to immunostaining with anti-Flag antibody and secondary Alexa fluor 594 donkey anti-mouse antibody (Molecular Probes, Eugene, OR) followed by counterstaining with DAPI (Thermofisher). Images were visualized by fluorescent microscopy (Carl Zeiss Axio Observer 7) using Zen Pro software.

In vivo ubiquitination assay

In vivo ubiquitination assays employed H1299 cells transfected with constructs as indicated using Lipofectamine 2000 (Invitrogen). MG132 (20 μM) was added 5 hours before harvesting. Cells were harvested 24 hours after transfection, and total cell lysates were prepared. For experiments using an HA-Ub construct, equal

amounts of cleared cell lysates were subjected to anti-p53 (FL393, Santa Cruz) or anti-Flag (M2, Sigma) immunoprecipitation followed by Western blotting with the monoclonal anti-HA antibody (BioLegend).

Cell proliferation assay

Cell proliferation was measured using the CellTiter 96® AQueous One Solution Cell Proliferation Assay (Promega) following the manufacturer's instruction. 1×10^5 U2OS cells per well were plated in 96-well plates. The cells in triplicates were then treated as indicated, and the plates were read 24 hours after treatment on a TECAN SPARK Microplate Reader (Tecan) at a wavelength of 490 nm. The results were expressed as means ± s.d. of three independent experiments.

Colony formation assay

Pooled isogenic U2OS cells were plated on 35 mm dishes or 12-well plates. The cells were treated with indicated drugs for 24 hours, and then fresh DMEM medium (without drug) was added and replaced every other day. Seven to fourteen days after treatment, the cells were fixed and stained with crystal violet (0.05% in 20% ethanol). The crystal violet stained cells were scanned using the LI-COR Odyssey CLx imaging system. The intensity of the crystal violet signal in each well was quantified to represent the cell numbers in the well. The signal of DMSO-treated wild-type cells were set as 100% for quantification.

Cell cycle analysis

U2OS cells were treated with 50 μM 5-FU for 24 hours and then harvested by trypsinization, fixed, and resuspended in Guava® Cell Cycle Reagent according to the manufacturer's instruction. Stained cells were analyzed with Guava® easyCyte™ Flow Cytometer (Luminex). The percentage of G1 and S phase cells was quantified using Guava Cell Cycle Software.

Glycolytic rate assay

25,000 cells were plated in Seahorse XFp cartridges the day prior to analysis. Seahorse XFp Glycolytic Rate Assay was performed according to the manufacturer's protocol. Rate data analysis was normalized based on the post-assay DNA content.

RNA extraction and quantitative RT-PCR analysis

RNA was extracted using a Qiagen RNeasy mini-kit, and cDNA was synthesized with the QuantiTect reverse transcription kit (Qiagen). Samples were analyzed by quantitative real-time PCR on a Bio-Rad CFX 96 using PowerUp SYBR Green (Thermo Fisher Scientific). RNA expression was normalized to RPL32 mRNA expression. Relative levels were calculated by the comparative Ct method (ΔΔCT method). The results are expressed as means ± s.d. of three experiments. Primer sequences are: RPL32, 5'-TTCCTGGTCCACAACGTCAAG-3' (Forward) and 5'-TGTGAGCGATCTCGGCAC-3' (Reverse); p21 (CDKN1A), 5'-GGCGGCAGACCAGCATGACA-3' (Forward) and 5'-GCAGGGGGCGGCCAGGGTAT-3' (Reverse); PUMA, 5'-CCTGGAGGGTCCTGTACAATCT-3' (Forward) and 5'-GCACCTAATTGGGCTCCATCT-3' (Reverse); TIGAR, 5'-CCAGGCTCGCAGCTTCA-3' (Forward) and 5'-GGTTTCGACTCCAGGTGCAA-3' (Reverse). Primers for C6orf15 (Forward: 5'-ACGATAGAGGGAAACCCAAC-3'; Reverse: 5'-TAGTGCTGGAAACATGCTGA-3'), COL3A1 (Forward: 5'-AGCTACGGCAATCCTGAACT-3'; Reverse: 5'-GGGCCTTCTTTACATTTCCA-3'), MMP9 (Forward: 5'-CTCTGGAGGTTCGACGTG-3'; Reverse: 5'-GTCCACCTGGTTCAACTCAC-3'), RAB11FIP4 (Forward: 5'-ACAGAGTCAGCAGGGAACTG-3'; Reverse: 5'-TCAGGAAACAGACCAGAAGC-3'), and TGM2 (Forward: 5'-GTCTGTGCACAAATCCATCA-3'; Reverse: 5'-CCAGTTTGTTCAGGTGGTTC-3') were obtained from RealTimePrimers.com.

RNA-sequencing

Two rounds of RNA sequencing were carried out with two different vendors. First, RNA from U2OS WT_1, WT_2, MUT_1, and MUT_2 cells was extracted using a Qiagen RNeasy mini-kit. RNA was then sent to Sulzberger Columbia Genome Center for standard STRPOLYA 40 m 2×100 bp Illumina NOVA sequencing. Second, RNA from U2OS WT_1, WT_2, MUT_1, and MUT_2 cells was extracted using a Qiagen RNeasy mini-kit. RNA was then sent to Azenta Life Sciences/GENEWIZ for standard STRPOLYA 40 m 2×150 bp Illumina NOVA sequencing. The fastq files for all samples were mapped to the human genome library (HG19), and TPMs were combined for the bioinformatics analysis. mRNA sequencing data has been depos-

Table 1. MDM2 mutations at residues that were shown to be critical to RPL11 interaction in COSMIC database

Sample Name	AA Mutation	Zygosity	Somatic Status	p53 mutation	Tumor type
TCGA-5L-AAT1-01	E292K	Unknown	Confirmed Somatic	WT	Breast Carcinoma
T2257	D294Y	Unknown	Confirmed Somatic	WT	Large intestine Carcinoma
TCGA-AB-2952-03	E296D	Heterozygous	Unknown	E286G	Acute myeloid leukaemia
46M	D301N	Unknown	Confirmed Somatic	WT	Malignant melanoma
PARXMV	C319R	Unknown	Confirmed Somatic	WT	Acute lymphoblastic T cell leukaemia
P-0010030-T01-IM5	C322Y	Heterozygous	Confirmed Somatic	WT	Lung Adenocarcinoma
P-0000791-T01-IM3	W323S	Heterozygous	Confirmed Somatic	WT	Germ cell tumour (testis)
GCYC_366_T	W323L	Unknown	Confirmed Somatic	R273C	Stomach Carcinoma
16710	W329G	Heterozygous	Confirmed Somatic	WT	Lung cancer
5-VS076-T1	W329L	Heterozygous	Confirmed Somatic	I255F, A161D	Colon cancer
TCGA-AJ-A3EK-01	W329C	Unknown	Confirmed Somatic	R213*	Endometrioid carcinoma

Three groups of residues were reported [33] to be critical to MDM2's binding to RPL11 based on the crystal structure of the MDM2-RPL11 complex: residues (colored green) that are important for zinc finger fold (C305, C308, C319, C322, W323 and H318); residues (colored blue) that form a charged surface in the acidic domain to establish an electrostatic interaction with RPL11 (E292, E293, D294, E296, and D301), and residues (colored red) that form hydrogen-bonding networks with the center of the palm of RPL11 (S317, W329, and N328). Sample information was retrieved from COSMIC database (https://cancer.sanger.ac.uk/cosmic). * indicates a nonsense substitution.

ited to the Gene Expression Omnibus (GEO), and access number is GSE267150.

Bioinformatics analysis

Differential gene expression analysis was provided by vendors using the standard DESeq2 analysis package [37]. Gene Set Enrichment Analysis (GSEA) was conducted as described [38] and implemented in the desktop module (http://www.gsea-msigdb.org/gsea/index.jsp) using previously reported cell cycle phase-specific gene sets [39]. DAVID version 6.7 (https://david.ncifcrf.gov/) was used to classify the functional categories, including KEGG pathway and gene ontology (GO) annotation enrichment analysis of differentially expressed proteins (DEPs) [40]. The gene lists were provided in Table S1.

Results

Cancer-associated MDM2 W329G mutant retained its binding to p53 and MDMX but reduced its interaction with RPL11

The center region of MDM2 has been shown to provide binding sites for many MDM2-interacting proteins, including ribosomal proteins. Three groups of residues were reported to be critical to MDM2's binding to RPL11 based on the crystal structure of the MDM2-RPL11 complex: residues that are important for zinc finger fold (C305, C308, C319, C322, W323 and H318); residues that form charged surface in the acidic domain to establish an electrostatic interaction with RPL11 (E292, E293, D294, E296, and D301), and residues that form hydrogen-bonding networks with the center of the palm of RPL11 (S317, W329, and N328) [30]. In the COSMIC dataset (to date), somatic mutations were found in 8 of these 14 residues, implying the physiologic importance of the MDM2/RPL11 interaction in tumor suppression (**Table 1**). When we initiated our study, we noticed that multiple patient samples contained MDM2 mutation at Trp329, including one with an MDM2 W329G mutation occurring in the wild-type p53 background. To confirm that W329G mutation affects the function of MDM2, we first examined the properties of MDM2 W329G mutant with ectopically expressed MDM2 W329G proteins. A co-immunoprecipitation assay revealed that MDM2 W329G retained its ability to bind to p53 (**Figure 1A**) and MDMX (**Figure 1B**). Note that the reduced levels of MDMX in the presence of wild-type MDM2 or MDM2 W329G but not MDM2 C462A (an E3 ligase defective MDM2 variant) indicated that MDM2 W329G retained its ability to degrade MDMX (**Figure 1B**). Consistent with the previous report that Trp329 is involved in MDM2-RPL11 interaction [30], MDM2 W329G was defective in interaction with RPL11 like C305F mutant, an MDM2 variant that was shown to lose the ability to bind to RPL11 [21] (**Figure 1C**). On the other

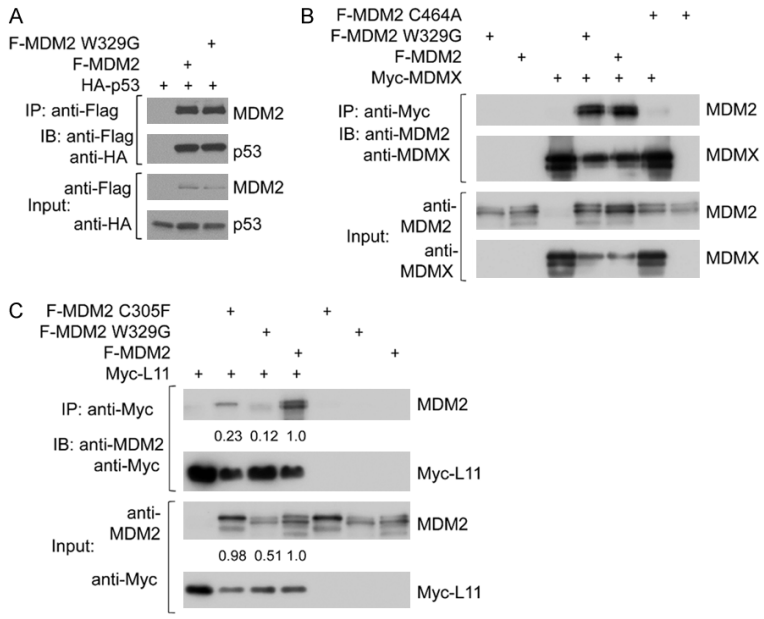

Figure 1. Cancer-associated MDM2 W329G mutant retained its binding to p53 and MDMX but not RPL11. A. MDM2 W329G retained its ability to interact with p53. 1.2 μg of Flag-tagged MDM2 (wild-type or W329G) were transfected with 0.3 μg of HA-p53 into H1299 cells. Twenty hours after transfection, cells were treated with MG132 (25 μM) for 4 hours. Then the cells were harvested, and total cell lysates were prepared. 200 μg of cell lysates were subjected to immunoprecipitation using anti-Flag antibody followed by immunoblotting with anti-Flag and anti-HA antibodies. 10% of total lysates were blotted as input control. B. MDM2 W329G retained its binding to MDMX. 1.2 μg of Flag-tagged MDM2 (wild-type, W329G, or C464A) were transfected with 0.3 μg of Myc-MDMX into H1299 cells. Twenty hours after transfection, cells were harvested, and total cell lysates were prepared. 200 μg of cell lysates were subjected to immunoprecipitation using anti-Myc antibody, followed by immunoblotting with anti-MDM2 and anti-MDMX antibodies. 10% of total lysates were blotted as input control. C. MDM2 W329G was defective in RPL11 binding. 1.2 μg of Flag-tagged MDM2 (wild-type, W329G, or C305F) were transfected with 0.5 μg of Myc-RPL11 into H1299 cells. Twenty hours after transfection, cells were harvested, and total cell lysates were prepared. 200 μg of cell lysates were subjected to immunoprecipitation using anti-Myc antibody, followed by immunoblotting with anti-MDM2 and anti-Myc antibodies. 10% of total lysates were blotted as input control. MDM2 blots for both input and co-immunoprecipitated samples were quantified using ImageJ software. The band intensity for wild-type Flag-MDM2 was set as 1.0, and the relative levels of MDM2 W329G and C305F were quantified accordingly.

hand, MDM2 W329G retained its binding to ribosomal protein S7 (RPS7) and p14/Arf, two other proteins shown to interact with MDM2 at the central region (data not shown).

MDM2 W329G mutant retained its E3 ligase activity but had an attenuated response to inhibition by RPL11

To examine whether MDM2 W329G mutation affects MDM2 stability, we transfected Flag-tagged wild-type or mutant MDM2 into U2OS cells with or without MG132 treatment 4 hours before harvesting. As shown in **Figure 2A**, the MDM2 W329G mutant was stabilized by MG132, similarly to wild-type MDM2. In line with this observation, we found that the MDM2 W329G mutant retained its ability to autoubiquitinate (**Figure 2B**) and exhibited similar subcellular localization as wild-type MDM2 when overexpressed and visualized by immunofluorescent staining (**Figure 2C**). In addition, when co-transfected with ectopic p53 in U2OS cells, the MDM2 W329G mutant retained its ability to degrade ectopically expressed p53 (**Figure 2D**). Consistent with its defect on RPL11 interaction, the inhibitory effect of RPL11 on MDM2-mediated p53 degradation was significantly attenuated for the MDM2 W329G mutant (**Figure 2D**). A p53-ubiquitination assay further confirmed that MDM2 W329G was capable of ubiquitinating p53 as wild-type MDM2 and RPL11 could inhibit its E3 ligase activity toward p53 much less efficiently compared to that of wild-type MDM2 (**Figure 2E**).

Cell lines with W329G mutation at endogenous MDM2 locus exhibited attenuated p53 response upon ribosomal stress stimuli treatment

To better understand mutant MDM2 function under a physiological setting, we established U2OS cell lines with MDM2 W329G mutation at its endogenous locus using CRISPR/Cas9-based genome editing method. Using our engineered isogenic cell lines, we found that endogenous MDM2 W329G, like ectopically expressed protein, retained its binding to p53 and MDMX (**Figure 3A**) and was defective on RPL11 upon 5-FU treatment (**Figure 3B**). As the RP-MDM2-p53 surveillance network serves as a crucial tumor-suppression mechanism, we

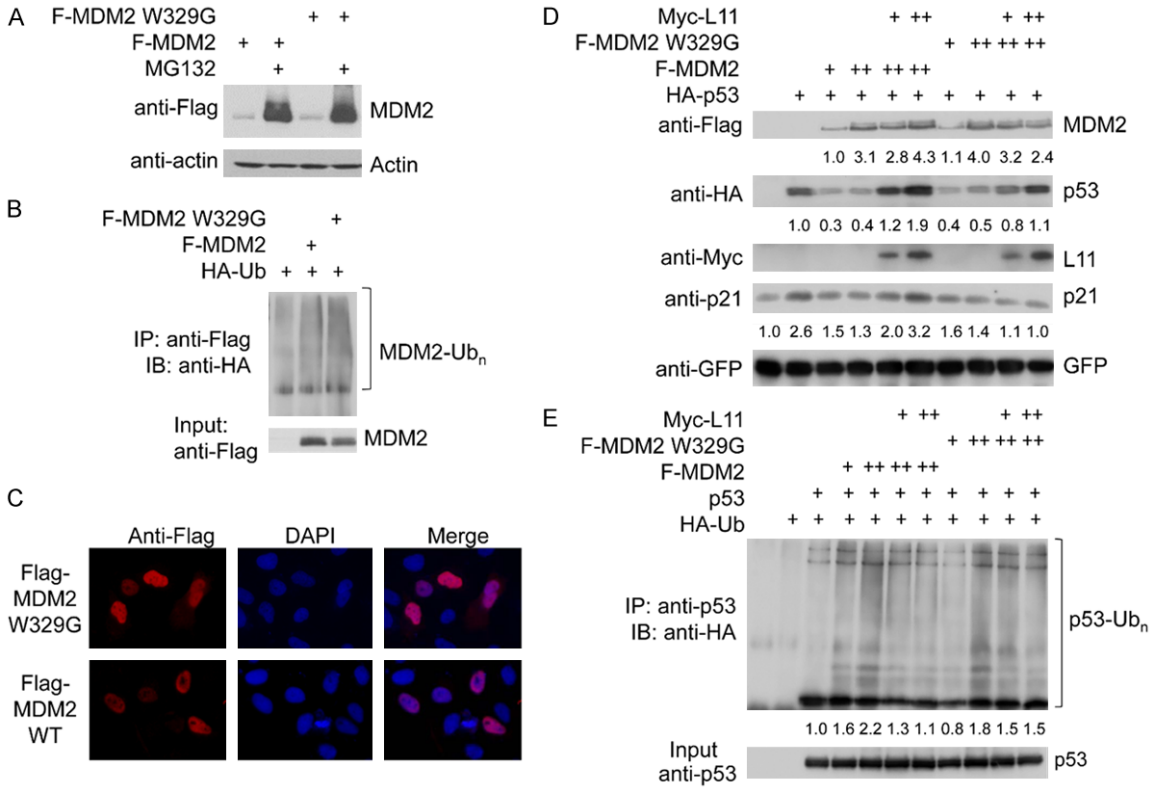

Figure 2. MDM2 W329G mutant retained its E3 ligase activity but had an attenuated response to RPL11 inhibition. A. MDM2 W329G was stabilized by MG132. 1.2 μg of Flag-tagged MDM2 (wild-type or W329G) was transfected into U2OS cells. Twenty hours after transfection, transfected cells were treated with or without MG132 (20 μM) for an additional 4 hours. Cells were then harvested, and total cell lysates were prepared and subjected to immunoblotting with anti-Flag or anti-actin antibodies. B. MDM2 W329G retained its auto-ubiquitination capacity. H1299 cells were transfected with 1.2 μg of HA-Ubiquitin together with Flag-tagged MDM2 (wild-type or W329G; 1.5 μg) as indicated. Twenty hours after transfection, cells were treated with MG132 (20 μM). Five hours later, cells were harvested, and total cell lysates were prepared. 200 μg of cell lysates were subjected to immunoprecipitation using anti-Flag antibody followed by immunoblotting with anti-HA antibodies. 10% of total lysates were blotted with anti-Flag antibody as input control. C. MDM2 W329G retained its nuclear localization as wild-type MDM2. 1 μg of Flag-tagged MDM2 (wild-type or W329G) was transfected into U2OS cells. Twenty-four hours after transfection, cells were fixed by 4% paraformaldehyde in PBS, then subjected to immunostaining with anti-Flag antibody, counterstained with DAPI, and visualized by fluorescence microscopy (Carl Zeiss). D. MDM2 W329G retained its ability to degrade p53 but resisted RPL11's inhibitory effect on MDM2-mediated p53 degradation. U2OS cells were transfected with a combination of plasmids (0.3 μg of HA-p53, 1 or 2 μg of Flag-tagged MDM2 variants, and 0.25 or 0.5 μg of Myc-L11) as indicated. pe-GFP N1 plasmid was also transfected as a transfection control. Twenty-four hours after transfection, cells were harvested, and total cell lysates were prepared and subjected to immunoblotting with anti-Flag, anti-HA, anti-p21, and anti-GFP antibodies. MDM2, p53, and p21 blots were quantified using ImageJ software. Relative band intensity was calculated accordingly, as indicated. E. MDM2 W329G resisted RPL11's inhibitory effect on MDM2-mediated p53 ubiquitination. H1299 cells were transfected with a combination of plasmids (1.2 μg of HA-Ub, 0.3 μg of untagged p53, 1 or 2 μg of Flag-tagged MDM2 variants, and 0.25 or 0.5 μg of Myc-L11) as indicated. Twenty hours after transfection, cells were treated with MG132 (20 μM). Five hours later, cells were harvested, and total cell lysates were prepared. 200 μg of cell lysates were subjected to immunoprecipitation using an anti-p53 (FL393) antibody, followed by immunoblotting with an anti-HA antibody. 10% of total lysates were blotted with anti-p53 antibody as input control. Ubiquitinated p53 species in the top panel were quantified using ImageJ software. Relative band intensity was calculated accordingly, as indicated.

examined the effect of W329G mutation on ribosomal stress-induced p53 response. As shown in **Figure 3C** and Figure S1A, homogenous U2OS W329G cell lines showed reduced p53 induction upon 5-FU (50 μM) or actinomycin D (5 nM) treatment compared to their wild-type counterparts. In line with that, the induction of p21 was attenuated in U2OS W329G cells. Note that it has been well-established that both 5-FU (50 μM) and actinomycin D (5

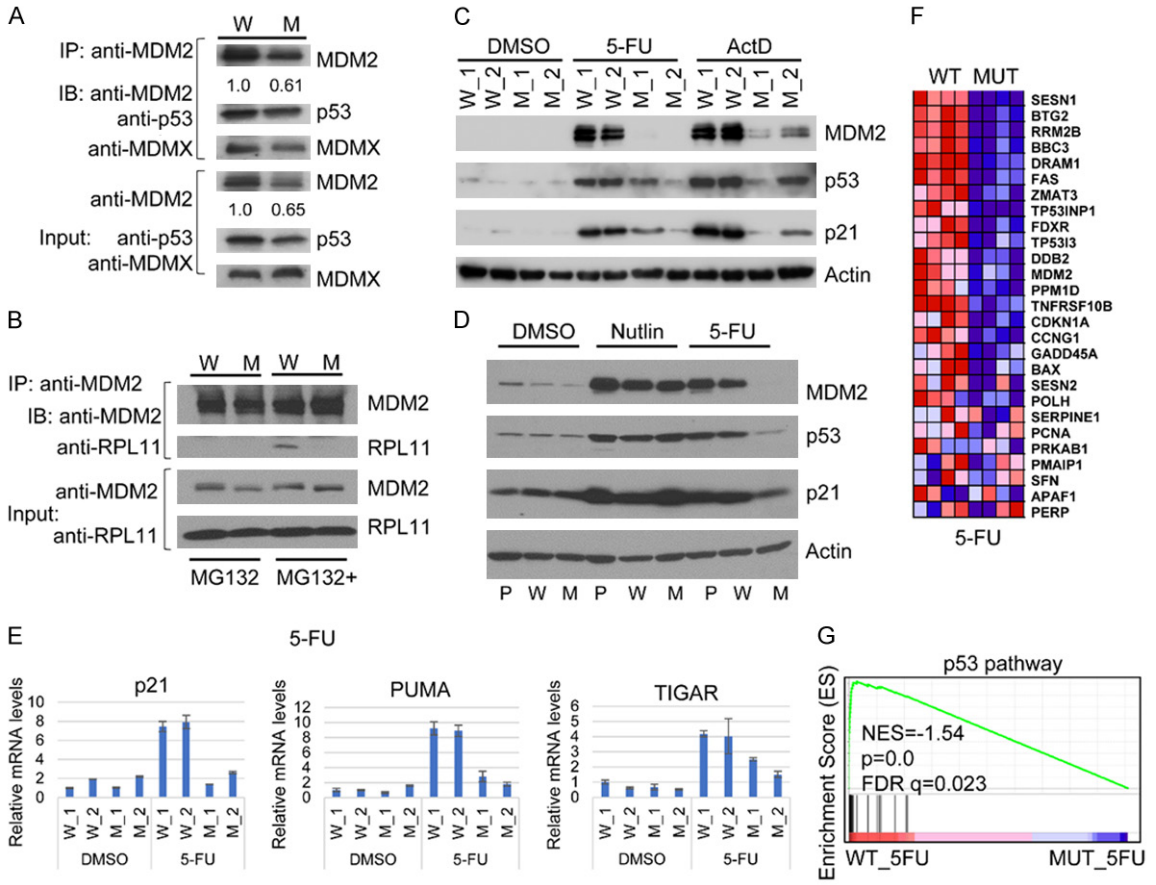

Figure 3. U2OS MDM2 W329G cells exhibited attenuated p53 response upon ribosomal stress stimuli treatment. A. Endogenous MDM2 W329G retained its ability to interact with endogenous p53 and MDMX. Total cell lysates (650 μg) from isogenic U2OS wild-type (W) or MDM2 W329G mutant (M) cells were subjected to immunoprecipitation using an anti-MDM2 (N-20) antibody, followed by immunoblotting with anti-MDM2, anti-p53, and anti-MDMX antibodies. 10% of total lysates were also blotted as input control. B. Endogenous MDM2 W329G is defective in RPL11 binding upon 5-FU treatment. Isogenic U2OS wild-type (W) or MDM2 W329G mutant (M) cells were treated with MG132 (25 μM) alone or with 5-FU (50 μM) for 4 hours. Total cell lysates (350 μg) were subjected to immunoprecipitation using an anti-MDM2 (N-20) antibody, followed by immunoblotting with anti-MDM2 and anti-RPL11 antibodies. 20% of total lysates were blotted as input control. C. U2OS cell lines with MDM2 W329G mutation exhibited attenuated p53 activation in response to 5-FU and Actinomycin D treatment. Isogenic U2OS wild-type (W) or MDM2 W329G mutant (M) cells were treated with DMSO, 5-FU (50 μM) or Actinomycin D (ActD; 5 nM) for 24 hours. Total cell lysates were immunoblotted with anti-MDM2, anti-p53, anti-p21, and anti-actin antibodies. D. U2OS cell lines with MDM2 W329G mutation exhibit similar p53 activation as wild-type cells in response to Nutlin-3a treatment. U2OS parental (P), isogenic wild-type (W), or MDM2 W329G mutant (M) cells were treated with DMSO, Nutlin-3a (10 μM), or 5-FU (50 μM) for 24 hours. Total cell lysates were immunoblotted with anti-MDM2, anti-p53, anti-p21, and anti-actin antibodies. E. Quantitative RT-PCR analysis of p21, PUMA, and TIGAR mRNA levels in isogenic U2OS cells with or without 5-FU treatment. Isogenic U2OS wild-type (W_1 and W_2) or MDM2 W329G mutant (M_1 and M_2) cells were treated with DMSO or 5-FU (50 μM) for 24 hours. Total RNAs were extracted and subjected to Real-Time Quantitative Reverse Transcription PCR analysis for p21, PUMA, and TIGAR genes. The data showed the representative results from 3 independent experiments. F. 5-FU-mediated induction of high-confidence p53 target genes was attenuated in U2OS cell lines with MDM2 W329G mutation. Isogenic U2OS cells were treated as in B and subjected to RNA sequencing analysis. Heatmap depicts differential gene expression of canonical p53 target genes in U2OS cells (wild-type vs W329G) treated with 5-FU. Columns represented individual cell clones from two independent experiments. G. Gene Set Enrichment Analysis of RNA sequencing data using a gene list for the p53 signaling pathway.

nM) induce ribosomal stress response at the dosage used here [41]. In addition, our wild-type control cells that underwent the same selection process as the mutant cells behaved similarly to U2OS parental cells (Figure S1A and **Figure 3D**). On the contrary, Nutlin-3a (an MDM2 inhibitor that disrupts MDM2/p53 interaction; **Figure 3D**) and DNA damage agent

etoposide-induced p53 and p21 expression were not affected by MDM2 W329G mutation (Figure S1B, S1C). Quantitative RT-PCR revealed that mRNA levels of classical p53 target genes p21, PUMA, and TIGAR were significantly reduced in 5-FU treated MDM2 W329G cells compared to isogenic wild-type cells (**Figure 3E**). To assess the global transcriptional profiles of U2OS cells varying in MDM2 status treated with DMSO or 5-FU, we carried out RNA-sequencing (RNA-seq) for U2OS W329G cells and the isogenic wild-type cells. Although basal expression of high-confidence p53 target genes remained unchanged overall, the induction of those genes following 5-FU treatment was significantly decreased in U2OS W329G cells (**Figure 3F**). Gene Set Enrichment Analysis confirmed the reduced expression of p53 pathway genes in 5-FU treated U2OS W329G cells compared to wild-type cells (**Figure 3G**). Together, our results indicate that the MDM2 W329G mutant attenuates p53 response to ribosomal stress.

5-FU mediated repression of genes in cell cycle and DNA replication was diminished in W329G mutant containing cells

Besides the p53 signaling pathway, DAVID KEGG pathway analysis of RNA-seq data revealed that DNA replication and cell cycle were the most changed pathways comparing 5-FU treated U2OS W329G and isogenic wild-type cells (**Figure 4A**). Notably, 5-FU-mediated repression of select E2F family members (E2F1 and E2F2) and multiple minichromosome maintenance protein complex (MCM) members (MCM2, MCM3, MCM4, MCM5, and MCM7) was diminished in W329G mutant containing cells (Table S1). We carried out western blot analysis and confirmed that 5-FU treatment led to repression of E2F1 in U2OS wild-type but not MDM2 W329G cells (**Figure 4B**). Furthermore, depletion of p53 by siRNAs rescued the E2F1 repression in response to 5-FU treatment (**Figure 4B**, top panel), consistent with previous reports showing that E2F-mediated signaling is repressed in a p21-dependent manner in response to p53 induction [42, 43]. To strengthen our conclusion, we have also generated stable p53 knockdown wild-type or mutant cells using a lentiviral system (Figure S2). Similarly, we observed 5-FU-mediated E2F1 repression in shRNA-control wild-type cells but not in shRNA-control W329G cells, and this repression was abolished in shRNA_p53 cells regardless of MDM2 status (**Figure 4B**, bottom panel). In line with the essential regulatory roles of p53 and E2F in cell cycle progression, Gene Set Enrichment Analysis revealed that the expression of G1/S phase-specific genes [39] was significantly enriched in 5-FU treated U2OS W329G cells in comparison to 5-FU treated U2OS wild-type cells (**Figure 4C**). Similarly, enrichment of G2/M phase-specific genes [39] was observed in 5-FU treated U2OS W329G cells in comparison to wild-type cells (Figure S3). Together, these data suggest that the MDM2 W329G mutant may promote resistance to 5-FU-mediated cell cycle arrest by attenuating p53-mediated E2F repression.

U2OS cells with MDM2 W329G mutation at its endogenous locus were more resistant to cell growth inhibition induced by ribosomal stress and exhibited higher glycolytic rates upon 5-FU treatment

We next examined the functional consequences of the MDM2 W329G mutation that might be associated with tumorigenesis. We found that U2OS cells with MDM2 W329G mutation were more resistant to cell growth inhibition induced by 5-FU in both cell proliferation assay (**Figure 5A**) and colony formation assay (**Figure 5B**). p53 depletion by siRNAs (Figure S4A) or shRNA (Figure S4B) in wild-type and MDM2 W329G cells led to resistance to 5-FU-induced cell growth inhibition to a similar extent, suggesting the effect of MDM2 W329G is p53-dependent. Cell cycle analysis revealed that MDM2 W329G cells were more resistant to cell cycle arrest induced by 5-FU than isogenic wild-type cells (**Figure 5C**). Moreover, previous studies with MDM2 C305F mice suggested that the ribosomal protein-MDM2-p53 pathway plays a significant role in maintaining metabolic homeostasis [44]. As MDM2 W329G, like MDM2 C305F, is defective in RPL11 interaction, we tested if U2OS W329G cells have metabolic alteration. We observed that cellular glycolytic flux, as measured by proton efflux rate, was lower in U2OS W329G cells compared to wild-type cells. 5-FU treatment significantly reduced cellular glycolytic flux in

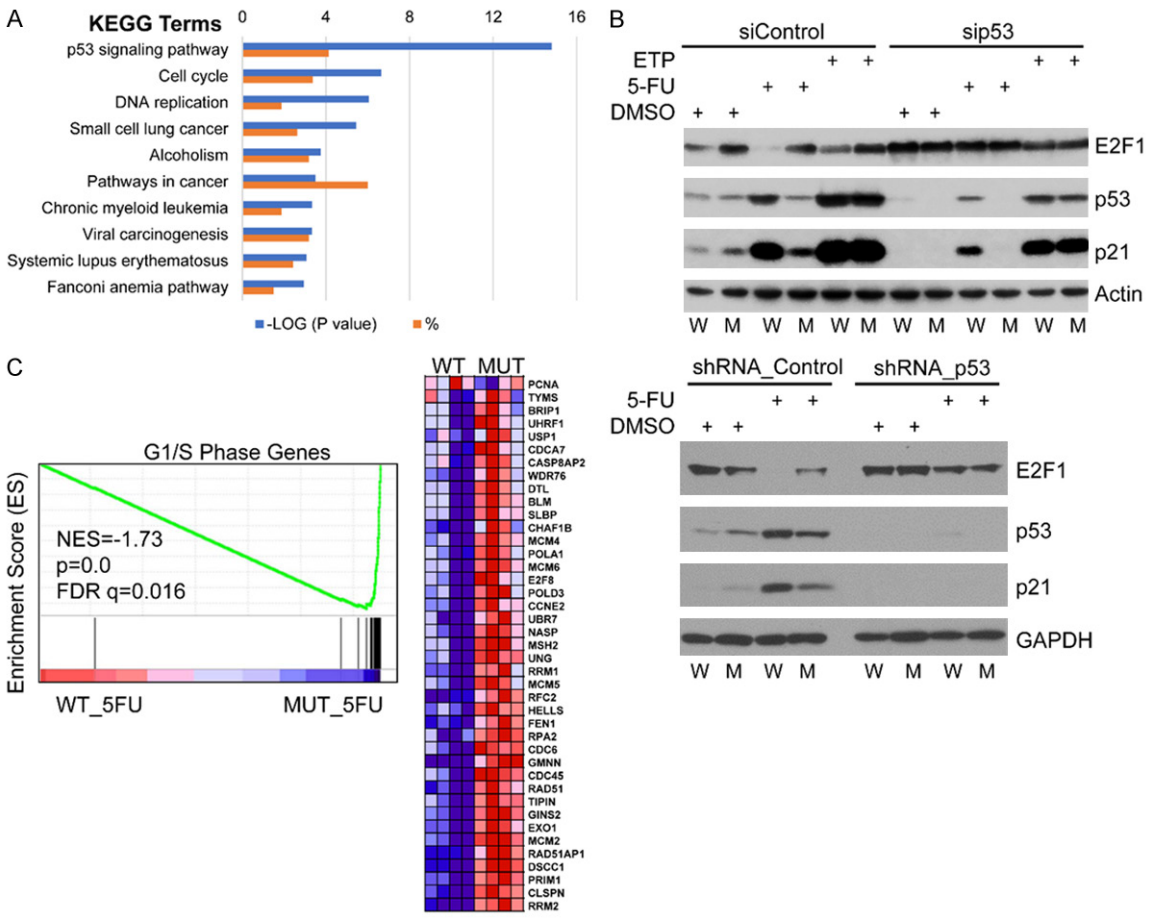

Figure 4. 5-FU mediated repression of genes in cell cycle and DNA replication was diminished in W329G mutant containing cells. A. KEGG pathway analysis of RNA sequencing data for 5-FU treated isogenic U2OS cells with wild-type or W329G MDM2. The top ten enriched pathways in U2OS wild-type cells compared to MDM2 W329G cells were ordered by *p*-value (blue) and % of differentially expressed genes (orange). B. 5-FU mediated repression of E2F1 was diminished in W329G mutant-containing cells. Top panel: a pool of isogenic U2OS cells (W: wild-type; M: W329G mutant) were plated and transfected with control siRNA or siRNAs targeting p53. Twenty-four hours after transfection, the cells were treated with DMSO, 5-FU (50 μM), or etoposide (ETP; 15 μM) for 24 hours. Cells were then harvested, and total cell lysates were subjected to immunoblotting with indicated antibodies. Bottom panel: a pool of stable shRNA_Control or shRNA_p53 U2OS cells (W: wild-type; M: W329G mutant) were treated with DMSO or 5-FU (50 μM) for 24 hours and total cell lysates were subjected to immunoblotting with indicated antibodies. C. Gene Set Enrichment Analysis of RNA sequencing data using a gene list for the G1/S phase of the cell cycle. Heatmap depicts differential gene expression of S phase genes in U2OS cells (wild-type vs W329G) treated with 5-FU. Columns represented individual cell clones from two independent experiments.

wild-type cells but much less in W329G cells (**Figure 5D**). The resistance of W329G cells to 5-FU-mediated reduction of glycolytic rate is most likely p53-dependent as p53-depleted wild-type and W329G cells exhibited similar glycolytic rate upon 5-FU treatment (**Figure 5D**).

U2OS cells with MDM2 W329G mutation at its endogenous locus had altered gene expression in extracellular matrix organization

Comparing the global transcription profile of U2OS cells with MDM2 W329G to that of isogenic wild-type U2OS cells without stress stimuli, we noticed limited numbers of significantly differentially expressed genes, consistent with the notion that MDM2 W329G largely retains its function (**Figure 6A**). Interestingly, gene ontology analysis revealed that a subgroup of those significantly differentially expressed genes was clustered in the extracellular matrix, extracellular region, and extracellular space (**Figure 6B**). Alterations in expression of those genes (C6orf15, COL3A1, MMP9, PAPPA2, RAB11FIP4, and TGM2), which have been documented to be involved in extracellular matrix

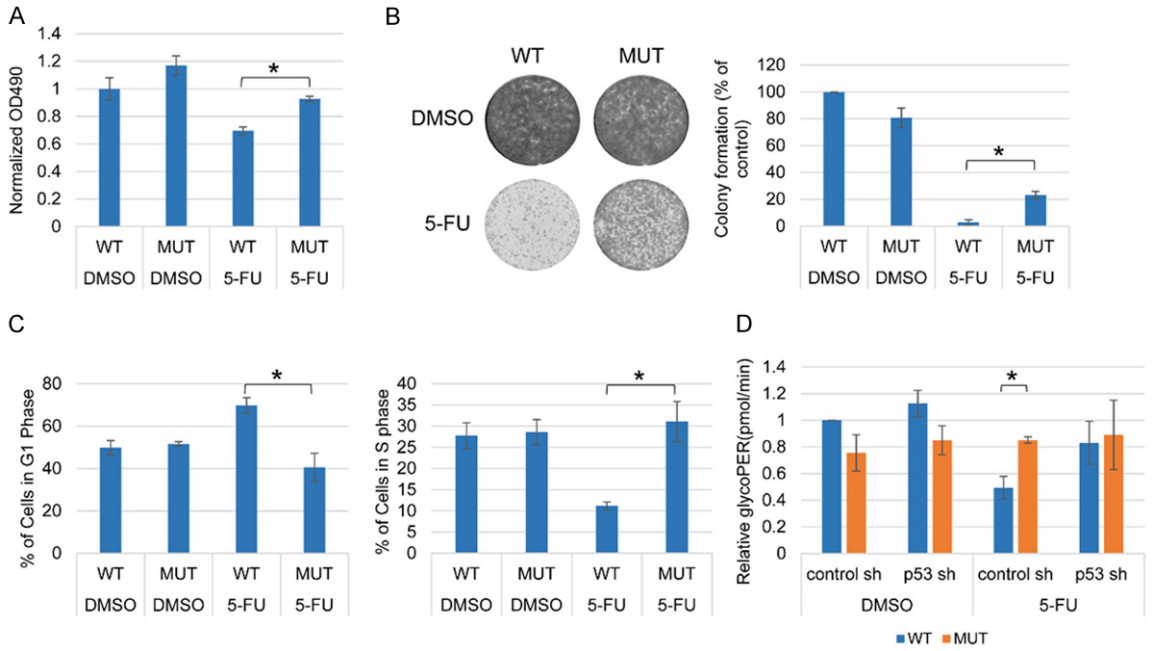

Figure 5. U2OS W329G cells were more resistant to cell growth inhibition induced by ribosomal stress and exhibited higher glycolytic rates upon 5-FU treatment. A. U2OS W329G cells were more resistant to 5-FU-induced cell proliferation inhibition. Pooled isogenic U2OS cells (wild-type; WT or W329G; MUT) were plated (1×10^5 cells/well) on 96-well plates in triplicates. After 24 hours, cells were treated with DMSO or 5-FU (50 μM) for 24 hours. Cell proliferation was measured as described in Materials and Methods. The results were expressed as means ± s.d. of three independent experiments. The asterisk indicates statistical significance (*P* value < 0.05). B. U2OS W329G cells were more resistant to 5-FU-induced cell growth inhibition. 2×10^4 pooled isogenic U2OS cells (wild-type; WT or W329G; MUT) were plated on 35 mm dishes. Twenty-four hours later, the cells were treated with DMSO or 5-FU (50 μM) for 24 hours. Fresh DMEM medium was then added to each dish and replaced every other day. The cells were fixed and stained 7 days after treatment. Relative colony formation capacity was quantified as described in Materials and Methods based on three independent experiments. The asterisk indicates statistical significance (*P* value < 0.05). C. U2OS W329G cells were more resistant to 5-FU-induced cell cycle arrest. Pooled isogenic U2OS cells (wild-type; WT or W329G; MUT) were treated with DMSO or 5-FU (50 μM) for 24 hours. Cell cycle analysis was performed as described in Materials and Methods. The percentage of cells in the G1 and S phases was plotted based on three independent experiments. The asterisk indicates statistical significance (*P* value < 0.05). D. U2OS W329G cells were more resistant to 5-FU-induced reduction of cellular glycolytic flux. 2.5×10^4 pooled isogenic shRNA_Control or shRNA_p53 U2OS cells (wild-type; WT or W329G; MUT) were plated on an Agilent Seahorse XFp cell culture miniplate and treated with DMSO or 5-FU (50 μM) for 24 hours. Cellular glycolytic flux was measured using Agilent Seahorse XFp Glycolytic Rate Assay Kit and analyzed with Agilent Seahorse XFp Glycolytic Rate Assay Report Generator. Rate data analysis was normalized based on the post-assay DNA content. The data were plotted based on three independent experiments. The asterisk indicates statistical significance (*P* value < 0.05).

organization and tumor progression, were maintained in 5-FU treated cells (**Figure 6C**). In addition, quantitative RT-PCR analysis of wild-type or mutant cells with or without p53 depletion by siRNAs revealed that the W329G mutation may affect the p53-independent function of MDM2. As shown in **Figure 6D** and Figure S5, the ratios of cellular levels of C6orf15, COL3A1, MMP9, RAB11FIP4, and TGM2 in mutant cells vs those in wild-type cells were maintained with or without p53 depletion. Together, these data suggested that W329G mutation may regulate extracellular matrix organization independent of p53.

Discussion

Although *MDM2* gene amplification/overexpression has been documented in various forms of cancer [15] and is the predominant alteration of the *MDM2* gene in tumor samples, mutation within functional domains of MDM2 may also contribute to its role in tumorigenesis. Advances in genome deep sequencing enable the identification of more somatic mutations and modifications of the cancer genome [19]. An increasing number of cancer-associated MDM2 mutations were listed in the Catalogue of Somatic Mutations in Cancer (COSMIC) data-

A

Summary of differentially expressed genes

Comparison	Upregulated Genes	Downregulated Genes	Total Significantly Differentially Expressed Genes
WT vs MUT (DMSO)	13	30	43
WT vs MUT (5-FU)	326	456	782

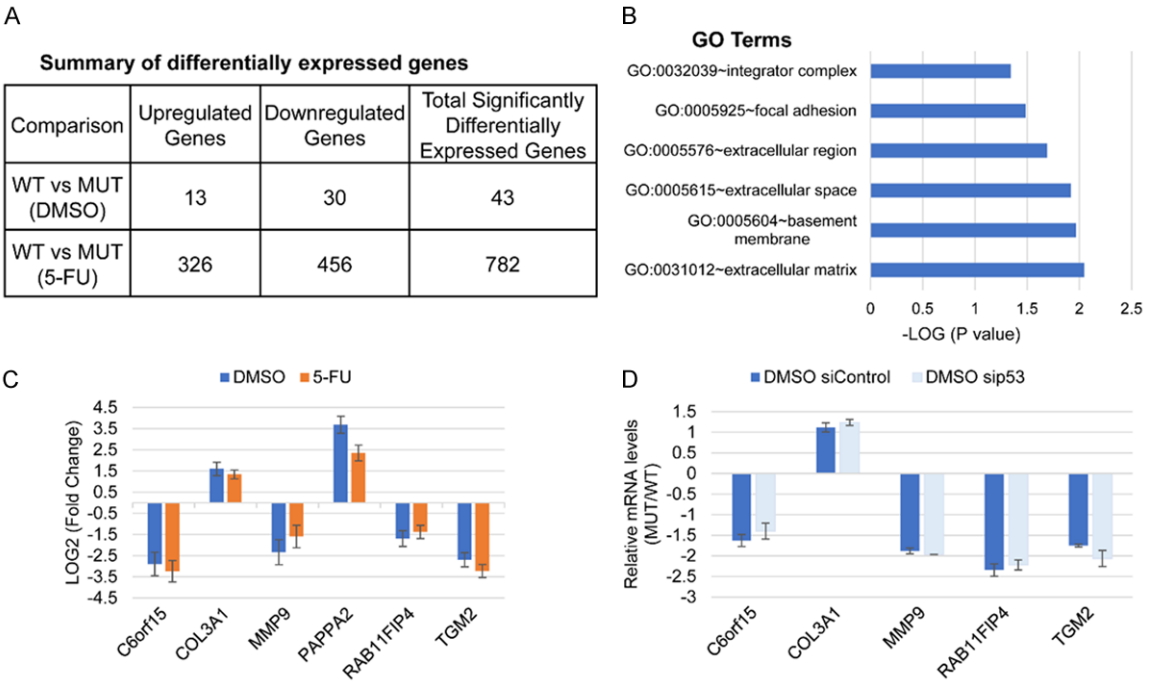

Figure 6. U2OS cells with MDM2 W329G mutation at their endogenous locus had altered gene expression in extracellular matrix organization. A. Summary of differentially expressed genes based on RNA sequencing analysis of DMSO or 5-FU treated isogenic U2OS cells. B. Gene Ontology analysis of RNA sequencing data for DMSO-treated isogenic U2OS cells with wild-type (WT) or W329G MDM2 (MUT). C. Differential gene expression of extracellular matrix organization genes in U2OS wild-type cells relative to W329G cells shown as log2 fold change. Data represent mean ± SEM for two independent clones in each treatment condition. D. Quantitative RT-PCR analysis of C6orf15, COL3A1, MMP9, RAB11FIP1, and TGM2 mRNA levels in isogenic U2OS cells with or without p53 depletion. Pools of isogenic U2OS wild-type (W_1 and W_2) or MDM2 W329G mutant (M_1 and M_2) cells were transfected with control siRNA or siRNAs targeting p53. Forty-eight hours after transfection, the cells were harvested, and total RNAs were extracted and subjected to Real-Time Quantitative Reverse Transcription PCR analysis for indicated genes. The ratios of relative expression levels of indicated genes in W329G mutant cells versus in wild-type cells were plotted. The data showed the representative results from 3 independent experiments.

base and The Cancer Genome Atlas (TCGA) database. Some mutations located at the functional domains of MDM2 are potentially oncogenic. Several cancer-associated MDM2 mutations, including W329G, have been characterized using ectopically overexpressed proteins. Mikawa et al. reported that cancer-associated M459I mutation diminished MDM2-mediated PGAM degradation in correlation with more cell transformation [23]. In that study, the M459I mutant was shown to be defective in both p53 and PGAM ubiquitination and degradation, but the W329G mutant was found to retain its E3 ubiquitin ligase activity to degrade p53 while being partially defective in PGAM ubiquitination. Chauhan et al. have selected multiple cancer-associated mutations in the p53 binding domain, acidic domain, zinc finger domain, and the RING domain of MDM2 and examined their effect on the abilities of MDM2 to interact and degrade p53 as well as MDM2 autoubiquitination with ectopically overexpressed proteins [24]. W329G was one of the mutants in their study that showed relatively similar activity as wild-type MDM2 in their ability to degrade p53. However, another mutation at Trp329 (W329L, identified in a patient with mutant p53) and the M459I mutation were found to promote p53 degradation. In our experimental system with overexpressed proteins, we also observed enhanced degradation of p53 by MDM2 M459I mutant (data not shown). Therefore, a cellular context-dependent differential regulation of MDM2 activity may be involved in studies with ectopically expressed MDM2 mutant proteins.

Here, consistent with those previous reports, we found that ectopically expressed MDM2 W329G mutant retained its ability to interact with, ubiquitinate, and degrade p53. In addition, we provided evidence showing that ectopically expressed MDM2 W329G mutant

retained the ability to interact with and degrade MDMX. In line with the notion that Trp329 is one of the residues involved in RPL11 interaction, as revealed in the crystal structure of the human MDM2-RPL11 complex [30], we found that MDM2 W329G variant was defective in RPL11 binding and resistant to the inhibition of RPL11 on MDM2-mediated p53 ubiquitination and degradation. Importantly, using cell lines with W329G mutation at the endogenous *MDM2* gene locus, we further demonstrated that MDM2 W329G mutant circumvents the ribosomal stress response to p53, promoting cell survival and glycolysis in a p53-dependent manner. Moreover, global gene expression profiling indicated that the MDM2 W329G mutant deregulates p53 function by altering p53 transcriptomes that are important for tumor suppression. In contrast to attenuated p53 signaling, W329G mutant-containing cells had elevated levels of select E2F family members (E2F1, E2F2, and E2F8) and MCM members (MCM2, MCM3, MCM4, MCM7, and MCM10) in comparison to wild-type cells upon 5-FU treatment. This is in line with the regulatory roles of p53 in the cell cycle and DNA replication. Although only one patient has the specific W329G mutation in the COSMIC database, we found that 11 cancer patients have MDM2 mutations on 8 out of 14 residues that were reported to be critical to MDM2/RPL11 interaction, and 7 MDM2 mutations occurred at wild-type p53 background (**Table 1**). This highlighted the importance of the RP-MDM2-p53 surveillance network in tumor suppression. Besides RPL11, a long list of ribosomal proteins has been similarly identified as MDM2-interacting proteins to inhibit MDM2 function. MDM2 residues that are responsible for their interactions haven't been thoroughly mapped. We would anticipate that more MDM2 mutations bypassing the RP signaling to p53 exist in cancer patients, which may pre-deposit and facilitate cancer formation and progression. Our study provided proof of concept that specific cancer-associated MDM2 mutations such as W329G may function as driver mutations for tumorigenesis through their ability to attenuate p53 response to stress stimuli. Accordingly, they may serve as biomarkers for cancer detection and precision therapy.

Even though p53 regulation is the best-characterized function of MDM2, evidence also supports a role for MDM2 in tumorigenesis that is independent of its effects on p53 [45]. MDM2 amplification/overexpression has been detected in various human cancers that lack p53 or have p53 mutations [46, 47]. Additionally, MDM2 splice variants lacking the p53 binding domain identified in tumors promote transformation *in vitro* despite their lack of p53 association [48]. Furthermore, mouse studies of MDM2 overexpression or heterozygous *MDM2* gene deletion have also revealed a p53-independent role for MDM2 in tumorigenesis [16, 49-51]. Moreover, MDM2 has noncarcinogenic roles in development, inflammation, tissue regeneration, and tissue remodeling that involve extracellular matrix organization [52-54]. Although we have been focused on the effect of MDM2 W329G on p53 regulation in the current study, comparing the global gene expression profile of wild-type cells to that of W329G mutant cells under unstressed conditions, our gene ontology analysis revealed the enrichment of genes in extracellular matrix, extracellular region, and extracellular space that have been shown be associated with malignant tumor progression. Expression alteration for those genes was maintained when cells were depleted of p53 or treated with 5-FU, suggesting that MDM2 W329G mutation deregulates the p53-independent function of MDM2, particularly on extracellular matrix modulation. Note that overexpression of C6orf15 [55], COL3A1 [56], MMP9 [57], PAPPA2 [58], RAB11FIP4 [59], and TGM2 [60] has been linked to and suggested as prognosis marker for various types of cancers. Particularly, MDM2 has been shown to regulate the expression of certain MMPs [61]. Correlation between the expression of MDM2 and MMP9 has been reported in human breast cancer [62], benzopyrene-induced lung cancer in rats [63], and pancreatic carcinoma SW1990HM cells [64]. Further studies will be needed to examine the potential regulatory roles of MDM2 on the expression of those extracellular matrix-associated genes and investigate the mechanistic basis of MDM2 W329G mutation on those intriguing functions of MDM2.

Acknowledgements

We are grateful to Dr. Carol Prives for helpful discussions and support. Ella Freulich and

Liang Lei are thanked for their expert technical assistance. This work is supported by NIH grant CA213426.

Disclosure of conflict of interest

None.

Address correspondence to: Dr. Yan Zhu, Department of Biological Sciences, St. John's University, Queens, NY 11439, USA. Tel: 718-990-3093; Fax: 718-990-5958; E-mail: zhuy1@stjohns.edu

References

[1] Oren M. Decision making by p53: life, death and cancer. Cell Death Differ 2003; 10: 431-442.
[2] Levine AJ. p53: 800 million years of evolution and 40 years of discovery. Nat Rev Cancer 2020; 20: 471-480.
[3] Klein AM, de Queiroz RM, Venkatesh D and Prives C. The roles and regulation of MDM2 and MDMX: it is not just about p53. Genes Dev 2021; 35: 575-601.
[4] Manfredi JJ. The Mdm2-p53 relationship evolves: Mdm2 swings both ways as an oncogene and a tumor suppressor. Genes Dev 2010; 24: 1580-1589.
[5] Wade M, Wang YV and Wahl GM. The p53 orchestra: Mdm2 and Mdmx set the tone. Trends Cell Biol 2010; 20: 299-309.
[6] Toledo F and Wahl GM. Regulating the p53 pathway: in vitro hypotheses, in vivo veritas. Nat Rev Cancer 2006; 6: 909-923.
[7] Shvarts A, Steegenga WT, Riteco N, van Laar T, Dekker P, Bazuine M, van Ham RC, van der Houven van Oordt W, Hateboer G, van der Eb AJ and Jochemsen AG. MDMX: a novel p53-binding protein with some functional properties of MDM2. EMBO J 1996; 15: 5349-5357.
[8] Gu J, Kawai H, Nie L, Kitao H, Wiederschain D, Jochemsen AG, Parant J, Lozano G and Yuan ZM. Mutual dependence of MDM2 and MDMX in their functional inactivation of p53. J Biol Chem 2002; 277: 19251-19254.
[9] Linares LK, Hengstermann A, Ciechanover A, Muller S and Scheffner M. HdmX stimulates Hdm2-mediated ubiquitination and degradation of p53. Proc Natl Acad Sci U S A 2003; 100: 12009-12014.
[10] Kawai H, Lopez-Pajares V, Kim MM, Wiederschain D and Yuan ZM. RING domain-mediated interaction is a requirement for MDM2's E3 ligase activity. Cancer Res 2007; 67: 6026-6030.
[11] Poyurovsky MV, Priest C, Kentsis A, Borden KL, Pan ZQ, Pavletich N and Prives C. The Mdm2 RING domain C-terminus is required for supramolecular assembly and ubiquitin ligase activity. EMBO J 2007; 26: 90-101.
[12] Wade M, Li YC and Wahl GM. MDM2, MDMX and p53 in oncogenesis and cancer therapy. Nat Rev Cancer 2013; 13: 83-96.
[13] Migliorini D, Lazzerini Denchi E, Danovi D, Jochemsen A, Capillo M, Gobbi A, Helin K, Pelicci PG and Marine JC. Mdm4 (Mdmx) regulates p53-induced growth arrest and neuronal cell death during early embryonic mouse development. Mol Cell Biol 2002; 22: 5527-5538.
[14] Parant J, Chavez-Reyes A, Little NA, Yan W, Reinke V, Jochemsen AG and Lozano G. Rescue of embryonic lethality in Mdm4-null mice by loss of Trp53 suggests a nonoverlapping pathway with MDM2 to regulate p53. Nat Genet 2001; 29: 92-95.
[15] Marine JC, Dyer MA and Jochemsen AG. MDMX: from bench to bedside. J Cell Sci 2007; 120: 371-378.
[16] Jones SN, Hancock AR, Vogel H, Donehower LA and Bradley A. Overexpression of Mdm2 in mice reveals a p53-independent role for Mdm2 in tumorigenesis. Proc Natl Acad Sci U S A 1998; 95: 15608-15612.
[17] Zhu Y, Wang H and Thuraisamy A. MDM2/P53 Inhibitors as Sensitizing Agents for Cancer Chemotherapy. Protein Kinase Inhibitors as Sensitizing Agents for Chemotherapy 2019.
[18] Konopleva M, Martinelli G, Daver N, Papayannidis C, Wei A, Higgins B, Ott M, Mascarenhas J and Andreeff M. MDM2 inhibition: an important step forward in cancer therapy. Leukemia 2020; 34: 2858-2874.
[19] Mardis ER. A decade's perspective on DNA sequencing technology. Nature 2011; 470: 198-203.
[20] Bond GL, Hu W, Bond EE, Robins H, Lutzker SG, Arva NC, Bargonetti J, Bartel F, Taubert H, Wuerl P, Onel K, Yip L, Hwang SJ, Strong LC, Lozano G and Levine AJ. A single nucleotide polymorphism in the MDM2 promoter attenuates the p53 tumor suppressor pathway and accelerates tumor formation in humans. Cell 2004; 119: 591-602.
[21] Lindstrom MS, Jin A, Deisenroth C, White Wolf G and Zhang Y. Cancer-associated mutations in the MDM2 zinc finger domain disrupt ribosomal protein interaction and attenuate MDM2-induced p53 degradation. Mol Cell Biol 2007; 27: 1056-1068.
[22] Macias E, Jin A, Deisenroth C, Bhat K, Mao H, Lindstrom MS and Zhang Y. An ARF-independent c-MYC-activated tumor suppression pathway mediated by ribosomal protein-Mdm2 interaction. Cancer Cell 2010; 18: 231-243.
[23] Mikawa T, Maruyama T, Okamoto K, Nakagama H, Lleonart ME, Tsusaka T, Hori K, Murakami I, Izumi T, Takaori-Kondo A, Yokode M, Pe-

ters G, Beach D and Kondoh H. Senescence-inducing stress promotes proteolysis of phosphoglycerate mutase via ubiquitin ligase Mdm2. J Cell Biol 2014; 204: 729-745.
[24] Chauhan KM, Ramakrishnan G, Kollareddy M and Martinez LA. Characterization of cancer-associated missense mutations in MDM2. Mol Cell Oncol 2016; 3: e1125986.
[25] Dolezelova P, Cetkovska K, Vousden KH and Uldrijan S. Mutational analysis reveals a dual role of Mdm2 acidic domain in the regulation of p53 stability. FEBS Lett 2012; 586: 2225-2231.
[26] Dolezelova P, Cetkovska K, Vousden KH and Uldrijan S. Mutational analysis of Mdm2 C-terminal tail suggests an evolutionarily conserved role of its length in Mdm2 activity toward p53 and indicates structural differences between Mdm2 homodimers and Mdm2/MdmX heterodimers. Cell Cycle 2012; 11: 953-962.
[27] Zhang Y and Lu H. Signaling to p53: ribosomal proteins find their way. Cancer Cell 2009; 16: 369-377.
[28] Golomb L, Volarevic S and Oren M. p53 and ribosome biogenesis stress: the essentials. FEBS Lett 2014; 588: 2571-2579.
[29] Iwakuma T and Lozano G. MDM2, an introduction. Mol Cancer Res 2003; 1: 993-1000.
[30] Zheng J, Lang Y, Zhang Q, Cui D, Sun H, Jiang L, Chen Z, Zhang R, Gao Y, Tian W, Wu W, Tang J and Chen Z. Structure of human MDM2 complexed with RPL11 reveals the molecular basis of p53 activation. Genes Dev 2015; 29: 1524-1534.
[31] Wang B, Gao J, Zhao Z, Zhong X, Cui H, Hou H, Zhang Y, Zheng J, Di J and Liu Y. Identification of a small-molecule RPL11 mimetic that inhibits tumor growth by targeting MDM2-p53 pathway. Mol Med 2022; 28: 109.
[32] Zhu Y, Poyurovsky MV, Li Y, Biderman L, Stahl J, Jacq X and Prives C. Ribosomal protein S7 is both a regulator and a substrate of MDM2. Mol Cell 2009; 35: 316-326.
[33] Trevino AE and Zhang F. Genome editing using Cas9 nickases. Methods Enzymol 2014; 546: 161-174.
[34] Kim JS, Lee C, Bonifant CL, Ressom H and Waldman T. Activation of p53-dependent growth suppression in human cells by mutations in PTEN or PIK3CA. Mol Cell Biol 2007; 27: 662-677.
[35] Xu A, Liu M, Huang MF, Zhang Y, Hu R, Gingold JA, Liu Y, Zhu D, Chien CS, Wang WC, Liao Z, Yuan F, Hsu CW, Tu J, Yu Y, Rosen T, Xiong F, Jia P, Yang YP, Bazer DA, Chen YW, Li W, Huff CD, Zhu JJ, Aguilo F, Chiou SH, Boles NC, Lai CC, Hung MC, Zhao Z, Van Nostrand EL, Zhao R and Lee DF. Rewired m(6)A epitranscriptomic networks link mutant p53 to neoplastic transformation. Nat Commun 2023; 14: 1694.
[36] Lee DF, Su J, Kim HS, Chang B, Papatsenko D, Zhao R, Yuan Y, Gingold J, Xia W, Darr H, Mirzayans R, Hung MC, Schaniel C and Lemischka IR. Modeling familial cancer with induced pluripotent stem cells. Cell 2015; 161: 240-254.
[37] Love MI, Huber W and Anders S. Moderated estimation of fold change and dispersion for RNA-seq data with DESeq2. Genome Biology 2014; 15: 550.
[38] Subramanian A, Tamayo P, Mootha VK, Mukherjee S, Ebert BL, Gillette MA, Paulovich A, Pomeroy SL, Golub TR, Lander ES and Mesirov JP. Gene set enrichment analysis: a knowledge-based approach for interpreting genome-wide expression profiles. Proc Natl Acad Sci U S A 2005; 102: 15545-15550.
[39] Tirosh I, Izar B, Prakadan SM, Wadsworth MH 2nd, Treacy D, Trombetta JJ, Rotem A, Rodman C, Lian C, Murphy G, Fallahi-Sichani M, Dutton-Regester K, Lin JR, Cohen O, Shah P, Lu D, Genshaft AS, Hughes TK, Ziegler CG, Kazer SW, Gaillard A, Kolb KE, Villani AC, Johannessen CM, Andreev AY, Van Allen EM, Bertagnolli M, Sorger PK, Sullivan RJ, Flaherty KT, Frederick DT, Jane-Valbuena J, Yoon CH, Rozenblatt-Rosen O, Shalek AK, Regev A and Garraway LA. Dissecting the multicellular ecosystem of metastatic melanoma by single-cell RNA-seq. Science 2016; 352: 189-196.
[40] Sherman BT, Hao M, Qiu J, Jiao X, Baseler MW, Lane HC, Imamichi T and Chang W. DAVID: a web server for functional enrichment analysis and functional annotation of gene lists (2021 update). Nucleic Acids Res 2022; 50: W216-W221.
[41] Sun XX, Dai MS and Lu H. 5-fluorouracil activation of p53 involves an MDM2-ribosomal protein interaction. J Biol Chem 2007; 282: 8052-8059.
[42] Benson EK, Mungamuri SK, Attie O, Kracikova M, Sachidanandam R, Manfredi JJ and Aaronson SA. p53-dependent gene repression through p21 is mediated by recruitment of E2F4 repression complexes. Oncogene 2014; 33: 3959-3969.
[43] Fischer M, Grossmann P, Padi M and DeCaprio JA. Integration of TP53, DREAM, MMB-FOXM1 and RB-E2F target gene analyses identifies cell cycle gene regulatory networks. Nucleic Acids Res 2016; 44: 6070-6086.
[44] Deisenroth C and Zhang Y. The ribosomal protein-Mdm2-p53 pathway and energy metabolism: bridging the gap between feast and famine. Genes Cancer 2011; 2: 392-403.
[45] Ganguli G and Wasylyk B. p53-independent functions of MDM2. Mol Cancer Res 2003; 1: 1027-1035.

[46] Cordon-Cardo C, Latres E, Drobnjak M, Oliva MR, Pollack D, Woodruff JM, Marechal V, Chen J, Brennan MF and Levine AJ. Molecular abnormalities of mdm2 and p53 genes in adult soft tissue sarcomas. Cancer Res 1994; 54: 794-799.

[47] Lu ML, Wikman F, Orntoft TF, Charytonowicz E, Rabbani F, Zhang Z, Dalbagni G, Pohar KS, Yu G and Cordon-Cardo C. Impact of alterations affecting the p53 pathway in bladder cancer on clinical outcome, assessed by conventional and array-based methods. Clin Cancer Res 2002; 8: 171-179.

[48] Sigalas I, Calvert AH, Anderson JJ, Neal DE and Lunec J. Alternatively spliced mdm2 transcripts with loss of p53 binding domain sequences: transforming ability and frequent detection in human cancer. Nat Med 1996; 2: 912-917.

[49] Alt JR, Greiner TC, Cleveland JL and Eischen CM. Mdm2 haplo-insufficiency profoundly inhibits Myc-induced lymphomagenesis. EMBO J 2003; 22: 1442-1450.

[50] McDonnell TJ, Montes de Oca Luna R, Cho S, Amelse LL, Chavez-Reyes A and Lozano G. Loss of one but not two mdm2 null alleles alters the tumour spectrum in p53 null mice. J Pathol 1999; 188: 322-328.

[51] Lundgren K, Montes de Oca Luna R, McNeill YB, Emerick EP, Spencer B, Barfield CR, Lozano G, Rosenberg MP and Finlay CA. Targeted expression of MDM2 uncouples S phase from mitosis and inhibits mammary gland development independent of p53. Genes Dev 1997; 11: 714-725.

[52] Ebrahim M, Mulay SR, Anders HJ and Thomasova D. MDM2 beyond cancer: podoptosis, development, inflammation, and tissue regeneration. Histol Histopathol 2015; 30: 1271-1282.

[53] Rathod J, Ismail S, Parmar M and Ray SD. Modulation of matrix metalloproteases (MMPs) AND MDM2 during acute dimethylnitrosamine (DMN)-induced nephrotoxicity in mice. The FASEB Journal 2007; 21: A810.

[54] Wang W, Qin JJ, Rajaei M, Li X, Yu X, Hunt C and Zhang R. Targeting MDM2 for novel molecular therapy: beyond oncology. Med Res Rev 2020; 40: 856-880.

[55] Hartung F, Wang Y, Aronow B and Weber GF. A core program of gene expression characterizes cancer metastases. Oncotarget 2017; 8: 102161-102175.

[56] Zhou J, Yang Y, Zhang H, Luan S, Xiao X, Li X, Fang P, Shang Q, Chen L, Zeng X and Yuan Y. Overexpressed COL3A1 has prognostic value in human esophageal squamous cell carcinoma and promotes the aggressiveness of esophageal squamous cell carcinoma by activating the NF-kappaB pathway. Biochem Biophys Res Commun 2022; 613: 193-200.

[57] Huang H. Matrix metalloproteinase-9 (MMP-9) as a cancer biomarker and MMP-9 biosensors: recent advances. Sensors (Basel) 2018; 18: 3249.

[58] Qin M, Liang Z, Qin H, Huo Y, Wu Q, Yang H and Tang G. Novel prognostic biomarkers in gastric cancer: CGB5, MKNK2, and PAPPA2. Front Oncol 2021; 11: 683582.

[59] He Y, Ye M, Zhou L, Shan Y, Lu G, Zhou Y, Zhong J, Zheng J, Xue Z and Cai Z. High Rab11-FIP4 expression predicts poor prognosis and exhibits tumor promotion in pancreatic cancer. Int J Oncol 2017; 50: 396-404.

[60] Huang L, Xu AM and Liu W. Transglutaminase 2 in cancer. Am J Cancer Res 2015; 5: 2756-2776.

[61] Bradbury R, Jiang WG and Cui YX. MDM2 and PSMA play inhibitory roles in metastatic breast cancer cells through regulation of matrix metalloproteinases. Anticancer Res 2016; 36: 1143-1151.

[62] Chen X, Qiu J, Yang D, Lu J, Yan C, Zha X and Yin Y. MDM2 promotes invasion and metastasis in invasive ductal breast carcinoma by inducing matrix metalloproteinase-9. PLoS One 2013; 8: e78794.

[63] Zhang DH, Zhang LY, Liu DJ, Yang F and Zhao JZ. Expression and significance of MMP-9 and MDM2 in the oncogenesis of lung cancer in rats. Asian Pac J Trop Med 2014; 7: 585-588.

[64] Shi W, Meng Z, Chen Z, Hua Y, Gao H, Wang P, Lin J, Zhou Z, Luo J and Liu L. RNA interference against MDM2 suppresses tumor growth and metastasis in pancreatic carcinoma SW1990HM cells. Mol Cell Biochem 2014; 387: 1-8.

Table S1. Functional Annotation Chart

Term	Count	%	*P*Value	Genes	List Tbtal	Pop Hits	Pop Total	Fold Enrichment	Bonferroni	Benjamini	FDR
hsa04115:p53 signaling pathway	22	4.11985	1.56E-15	CDKN1A, RRM2, CD82, GADD45A, TNFRSF10B, PPM1D, BBC3, DDB2, TP53I3, SESN3,CCNE2, RRM2B, CCNE1, ZMAT3, CCNG2, SESN1, CCNG1, SESN2, MDM2, FAS, BAX, TP73	249	73	8164	9.881058	4.27E-13	4.29E-13	4.09E-13
hsa04110:Cell cycle	18	3.370787	2.21E-07	CDKN1A, MCM7, GADD45A, CDC6, CDC25A, ORC6, CDC45, CCNE2, CCNE1, MYC, MDM2, MCM3, E2F1, MCM4, E2F2, MCM5, SKP2, MCM2	249	126	8164	4.683878	6.09E-05	3.04E-05	2.90E-05
hsa03030:DNA replication	10	1.872659	8.75E-07	POLD4, RFC4, MCM7, RFC2, PRIM1, MCM3, MCM4, MCM5, DNA2, MCM2	249	36	8164	9.107541	2.41E-04	8.02E-05	7.64E-05

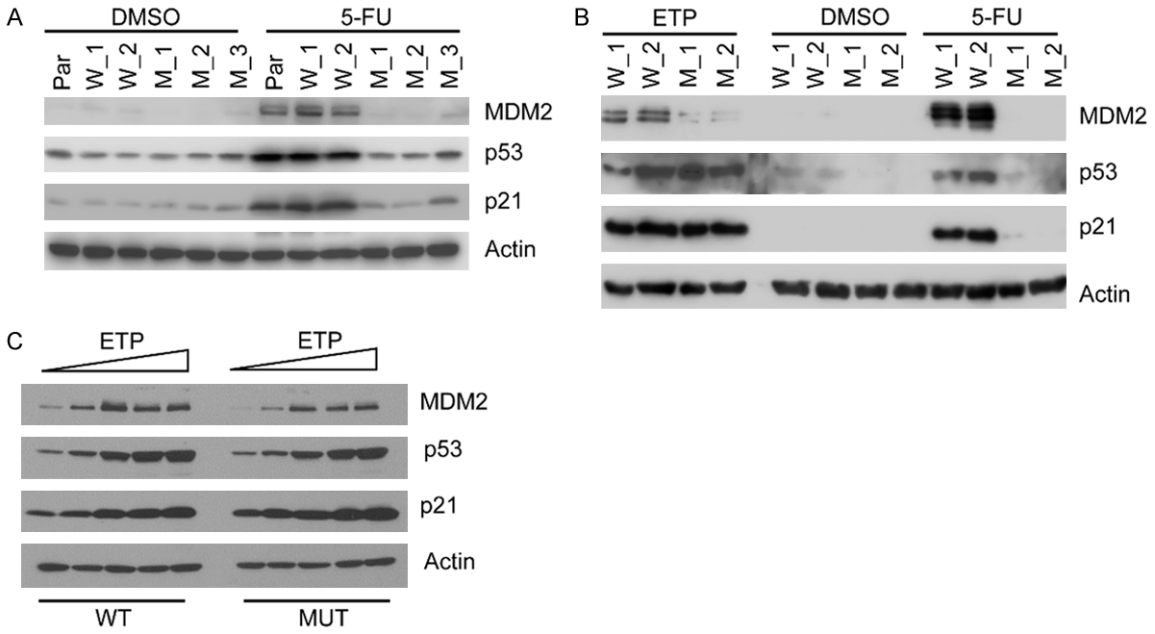

Figure S1. Etoposide-induced p53 and p21 expression were not affected by MDM2 W329G mutation. A. 5-FU-mediated p53 responses were attenuated in MDM2 W329G mutant cells but not in parental U2OS and isogenic U2OS wild-type cells. Parental U2OS cells and isogenic U2OS wild-type or MDM2 W329G mutant cells were treated with DMSO or 5-FU (50 μM). Total cell lysates were immunoblotted with anti-MDM2, anti-p53, anti-p21, and anti-actin antibodies. B. 5-FU but not etoposide-induced p53 and p21 expression was affected by MDM2 W329G mutation. Isogenic U2OS wild-type or MDM2 W329G mutant cells were treated with DMSO, 5-FU (50 μM), or etoposide (ETP; 15 μM) for 24 hours. Total cell lysates were immunoblotted with anti-MDM2, anti-p53, anti-p21, and anti-actin antibodies. C. MDM2 W329G mutation did not affect etoposide-induced p53 expression. A pool of isogenic U2OS wild-type (W) or MDM2 W329G mutant (M) cells were treated with DMSO or an increasing dosage of etoposide (ETP; 0.15, 1.5, 15, or 30 μM) for 24 hours. Total cell lysates were immunoblotted with anti-MDM2, anti-p53, anti-p21, and anti-actin antibodies.

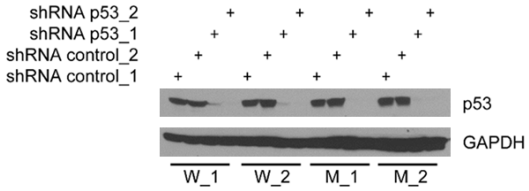

Figure S2. p53 knockdown in isogenic U2OS wild-type or MDM2 W329G mutant cells with a lentiviral shRNA system. Isogenic U2OS wild-type (W_1 and W_2) or MDM2 W329G mutant (M_1 and M_2) cells were infected with lentiviral particles containing shRNAs targeting p53 (pLKO-p53-shRNA-427/shRNA p53_1 and pLKO-p53-shRNA-941/shRNA p53_2) as well as control shRNAs (pLKO.pig Luc shRNA/shRNA control_1 and pLKO.pig control shRNA1/shRNA control_2) produced in HEK293T cells. 2 μg/ml of puromycin was added to the transduced plates two days after infection. Five days after selection, aliquots of cells were harvested, and total cell lysates were immunoblotted with anti-p53 and anti-GAPDH antibodies.

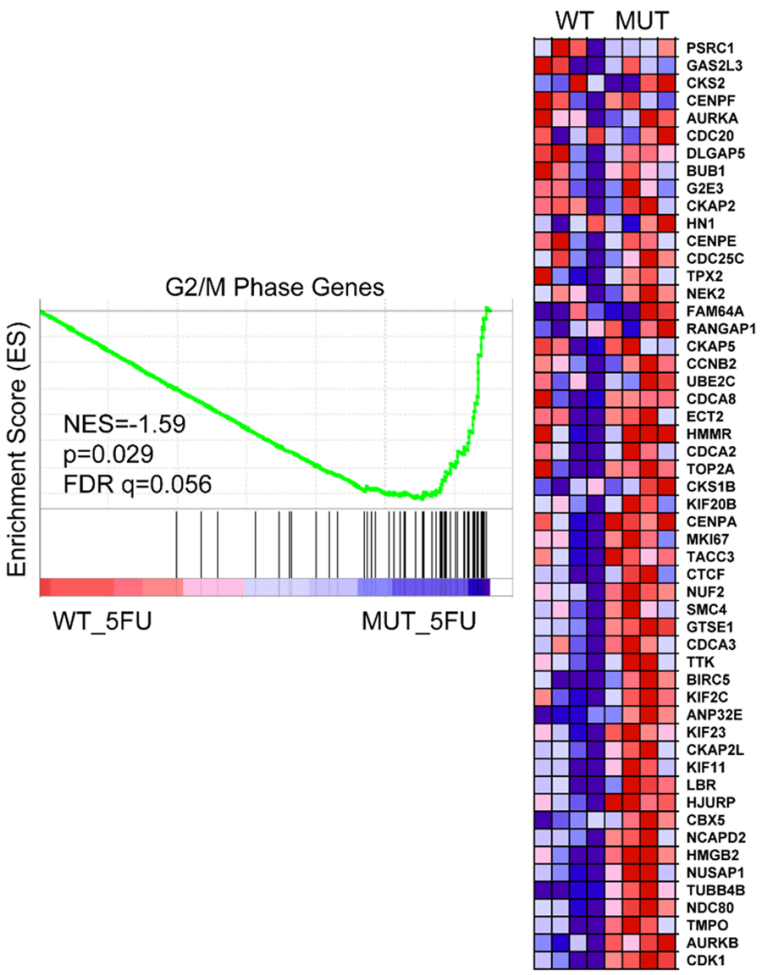

Figure S3. Gene Set Enrichment Analysis of RNA sequencing data using a gene list for the G2/M phase of the cell cycle. Heatmap depicts differential gene expression of G2/M phase genes in U2OS cells (wild-type vs W329G) treated with 5-FU. Columns represented individual cell clones from two independent experiments.

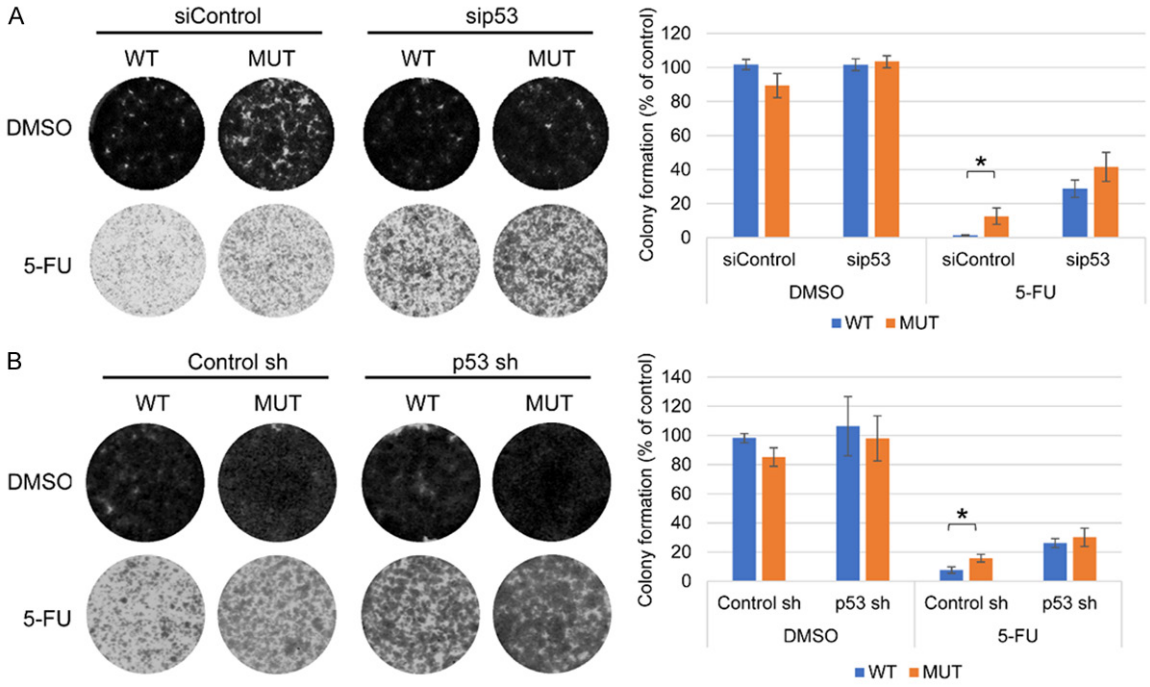

Figure S4. p53 depletion partially rescued 5-FU-mediated cell growth inhibition. A. Pooled isogenic U2OS cells (wild-type or W329G) were transfected with control siRNAs or siRNAs targeting p53. Twenty-four hours after transfection, cells were trypsinized and counted. 1×10^4 isogenic cells were plated on each well of a 12-well plate. Twenty-four hours later, the cells were treated with DMSO or 5-FU (50 μM) for 24 hours. Fresh DMEM medium (without 5-FU) was then added into each well and replaced every other day. The cells were fixed and stained 7 days after treatment. B. 8×10^3 pooled isogenic shRNA_Control or shRNA_p53 U2OS cells (wild-type; WT or W329G; MUT) were plated on each well of a 12-well plate. Twenty-four hours later, the cells were treated with DMSO or 5-FU (50 μM) for 24 hours. Fresh DMEM medium (without 5-FU) was then added into each well and replaced every other day. The cells were fixed and stained 14 days after treatment. Relative colony formation capacity was quantified as described in Materials and Methods based on three independent experiments. The asterisk indicates statistical significance (*P* value < 0.05).

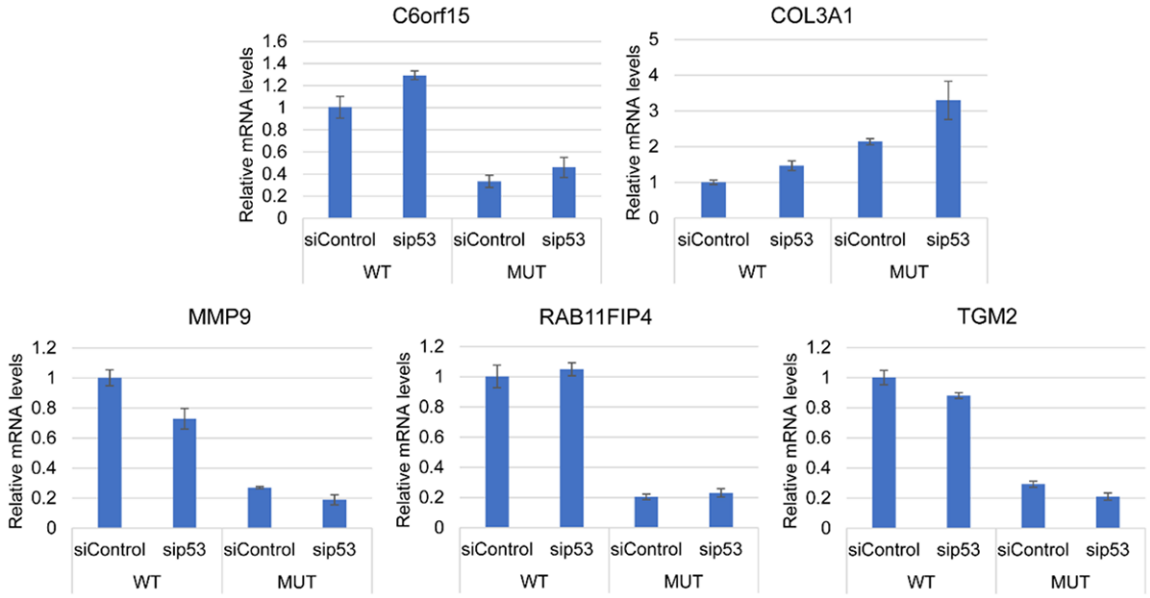

Figure S5. W329G mutation may regulate extracellular matrix organization independent of p53. Pools of isogenic U2OS wild-type (W_1 and W_2) or MDM2 W329G mutant (M_1 and M_2) cells were transfected with control siRNA or siRNAs targeting p53. Forty-eight hours after transfection, the cells were harvested, and total RNAs were extracted and subjected to Real-Time Quantitative Reverse Transcription PCR analysis for C6orf15, COL3A1, MMP9, RAB11FIP1, and TGM2 genes. The data showed the representative results from 3 independent experiments.